ASM Sc. J., 12, Special Issue 1, 2019 for IQRAC2018, 71-81

MHD Mixed Convective Stagnation Point Flow with Heat Generation Past a Shrinking Sheet

Najiyah Safwa Khashi'ie*[1,2], Norihan Md Arifin[1,3], Ezad Hafidz Hafidzuddin[4], and Nadihah Wahi[3]

[1]*Institute for Mathematical Research, Universiti Putra Malaysia, 43400 UPM Serdang, Selangor, Malaysia*
[2]*Fakulti Teknologi Kejuruteraan Mekanikal dan Pembuatan, Universiti Teknikal Malaysia Melaka, Hang Tuah Jaya, 76100 Durian Tunggal, Melaka, Malaysia*
[3]*Department of Mathematics, Faculty of Science, Universiti Putra Malaysia, 43400 UPM Serdang, Selangor, Malaysia*
[4]*Centre of Foundation Studies for Agricultural Science, Universiti Putra Malaysia, 43400 UPM Serdang, Selangor, Malaysia*

**Corresponding author: najiyah@utem.edu.my*

This paper investigates the influence of magnetohydrodynamics (MHD) mixed convective stagnation point flow over a shrinking sheet with the enhancement of heat generation/source. Using appropriate similarity transformations, the model are transformed into a system of nonlinear equations and then solved using bvp4c built-in-function in Matlab. Numerical results are presented graphically for the distributions of velocity, temperature as well as the skin friction coefficient and local Nusselt number. The findings revealed the dual solutions obtained within a particular range of the mixed convection parameter and shrinking parameter. It is found that the fluid velocity increases with the increasing values of the magnetic and mixed convection parameter while opposite results obtained for the fluid temperature. A stability analysis was performed and it is proven that the first solution is physically realizable and stable whereas the second solution is unstable.

Keywords: dual solutions, mixed convection, MHD, stagnation flow, shrinking sheet

I. Introduction

Stagnation point flow occurs at the surface of the bodies or object moving in a fluid. The stagnation or static pressure is at its maximum value at the stagnation point. Plane counterflow jet is one of the engineering applications that related to the stagnation flow. (Hiemenz, 1911) was first to study the stagnation point flow while (Homann, 1936) analyzed the axisymmetric case.

Stagnation point flow due to a stretching sheet was investigated by (Chiam, 1994), (Mahapatra and Gupta, 2001, 2002) while (Ishak et al., 2009) discussed the magnetohydrodynamics (MHD) stagnation point flow towards a stretching surface with varied surface temperature. This study found that heat transfer rate increased with the enhancement of magnetic parameter. Combination of both stagnation point flow and shrinking surface were studied by (Wang, 2008). Generally, solutions do not exist for a shrinking problem due to vorticity which could not be confined in the boundary layer. Wang found that with the addition of stagnation point flow to contain the vorticity, the non unique similarity solutions exist. The effect of magnetic field on stagnation point flow past a shrinking sheet have been analyzed by (Mahapatra et al., 2011) while (Fauzi et al., 2015) discovered the existance of dual solutions for stagnation point flow and heat transfer over a nonlinear shrinking sheet with slip effects. (Awaludin et al., 2016) extended and proved

Wang's work that dual solutions are exist for shrinking case while unique solution obtained for the stretching case. Stability analysis has been performed to determine the stable solution and its flow. (Rosali et al., 2011) considered the stagnation point flow in a porous medium showing that unique solution exist for stretching problem and dual solutions exist for shrinking problem.

(Ishak et al., 2006) considered the buoyancy effect for both assisting and opposing flow cases over stretching vertical sheet. He found that for the assisting flow case, both skin friction coefficient and local Nusselt number increased with the increment of the buoyancy parameter while for the opposing flow case, reverse results were obtained. (Ishak et al., 2008) investigated the buoyancy effect of a stagnation point flow on a vertical porous plate and discovered that dual solutions were possible on a certain range of non-dimensional parameter. (Pal, 2009) discussed the heat and mass transfer in stagnation point flow over a stretching sheet with the buoyancy force and thermal radiation. (Singh and Sharma, 2014) obtained dual solutions for the boundary layer flow along a vertical isothermal reactive plate near the stagnation point. (Ali et al., 2014) investigated MHD mixed convection of stagnation point flow on a vertical stretching sheet while (Shen et al., 2015) studied the MHD mixed convection stagnation point flow along a nonlinear vertical stretching sheet. Recently, (Seth et al., 2017) analyzed the effect of heat source and porous parameters on stagnation point flow and heat transfer past both stretching and shrinking sheets. They found that dual solutions for some cases of shrinking sheet while single solution for stretching sheet. Three dimensional mixed convection flow over stretching and shrinking surface have been considered by (Jamaludin et al., 2017). The findings revealed that the upper and lower branch solutions exist within a certain range of the mixed convection parameter, stretching/shrinking parameter, suction parameter and velocity slip parameter. (Sharma et al., 2018) investigated MHD mixed convection stagnation point flow over a linear stretching surface with the presence of heat source/sink. These study showed that the heat transfer rate increased with the increment of magnetic parameter while decrease with the increment of heat source parameter. In the present work, MHD mixed convective stagnation point flow of a viscous fluid towards a shrinking surface with the enhancement of heat source is considered. To the authors' best knowledge, no studies have been reported which discuss the present work.

II. Methodology

A steady, laminar, two-dimensional mixed convective stagnation point flow of an incompressible viscous fluid towards a shrinking sheet is considered. A uniform magnetic field, B_0 is applied normal to the sheet in order to stabilize the boundary layer with the presence of heat source. $U_w(x) = ax$ and $U_e(x) = bx$ are the stretching/shrinking velocity and free stream velocity respectively where $a > 0$ for stretching sheet, $a < 0$ for shrinking sheet and b is a positive constant as depicted in Fig. 1. Under the usual boundary layer approximations, the governing equations are given by:

$$\frac{\partial u}{\partial x} + \frac{\partial v}{\partial y} = 0, \tag{1}$$

$$u\frac{\partial u}{\partial x} + v\frac{\partial u}{\partial y} = U_e\frac{dU_e}{dx} + \nu\frac{\partial^2 u}{\partial y^2} - \frac{\sigma {B_0}^2}{\rho}(u - U_e) + g\beta_T (T - T_\infty), \tag{2}$$

$$u\frac{\partial T}{\partial x} + v\frac{\partial T}{\partial y} = \alpha\frac{\partial^2 T}{\partial y^2} + \frac{Q}{\rho C_p}(T - T_\infty), \tag{3}$$

with boundary conditions

$$\begin{gathered} u(x,0) = U_w(x), \qquad v(x,0) = 0, \\ T(x,0) = T_w(x), \\ u(x,y) \to U_e(x), \qquad T(x,y) \to T_\infty \\ \text{as} \quad y \to \infty \end{gathered} \tag{4}$$

where (u, v) are the velocity components along the (x, y) axes respectively, T is the fluid temperature, T_∞ is the free stream temperature,

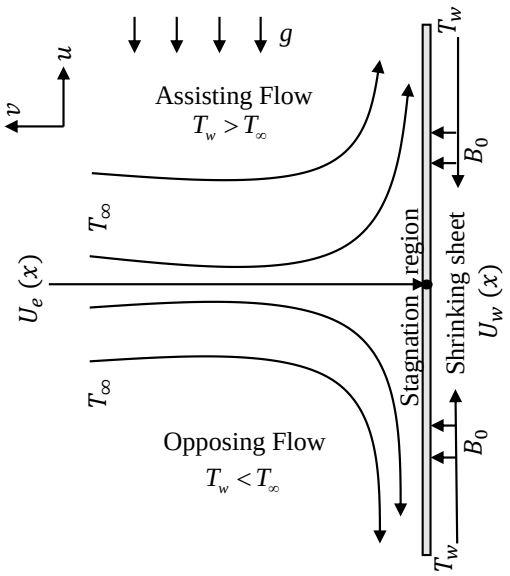

Figure 1: The physical model

ν is the kinematic viscocity, σ is the electrical conductivity of the fluid, ρ is the fluid density, g is the gravitational acceleration, β_T is the thermal expansion, α is the thermal diffusivity, Q is the dimensional heat generation coefficient and C_p is the specific heat of fluid. $T_w(x) = T_\infty + cx$ is the temperature of the sheet where assisting flow case (heated surface) denoted by $c > 0\,(T_w > T_\infty)$ while opposing flow case (cooled surface) denoted by $c < 0\,(T_w < T_\infty)$(Isa et al., 2017, Sharma et al., 2018).

A. Similarity Transformation

The following similarity transformation have been introduced to transform Eqs.(1)-(3) subject to the boundary conditions (4) into a system of ordinary differential equation

$$\eta = \sqrt{\frac{U_e}{\nu x}}y, \qquad f(\eta) = \frac{\psi}{\sqrt{U_e \nu x}}, \qquad \theta(\eta) = \frac{T - T_\infty}{T_w - T_\infty}, \tag{5}$$

where η is the similarity variable and ψ is the stream function such that

$$u = \frac{\partial \psi}{\partial y} \quad \text{and} \quad v = -\frac{\partial \psi}{\partial x}, \tag{6}$$

which satisfies (1). Using Eqs. (5) and (6),

$$u = bxf'(\eta) \quad \text{and} \quad v = -\sqrt{b\nu}f(\eta). \tag{7}$$

Hence, the transformed nonlinear ordinary differential equations are:

$$f''' + ff'' - \left(f'\right)^2 + M\left(1 - f'\right) + 1 + \lambda\theta = 0, \tag{8}$$

$$\frac{1}{Pr}\theta'' + f\theta' - f'\theta + S\theta = 0, \tag{9}$$

where primes denote differentiation with respect to similarity variable η, $M = \dfrac{\sigma {B_0}^2}{\rho b}$ is the magnetic field parameter, $\lambda = \dfrac{Gr_x}{Re_x^2}$ is the mixed convection or buoyancy parameter, $Gr_x = \dfrac{g\beta_T\left(T_w - T_\infty\right)x^3}{\nu^2}$ is the local Grashof number and $Re_x = \dfrac{xU_e(x)}{\nu}$ is the local Reynolds number. It should be noticed that λ is a constant, such that $\lambda > 0$ and $\lambda < 0$ represent assisting and opposing flows, correspondingly. Further, Pr$= \dfrac{\nu}{\alpha}$ is the Prandtl number and $S = \dfrac{Q}{\rho b C_p}$ is the heat generation coefficient. The corresponding boundary conditions are

$$\left.\begin{array}{l} f(0) = 0, \quad f'(0) = \varepsilon, \quad \theta(0) = 1 \\ f'(\eta) \to 1, \quad \theta(\eta) \to 0 \quad \text{as} \quad \eta \to \infty \end{array}\right\}, \tag{10}$$

where ε is the velocity ratio parameter ($\varepsilon > 0$ and $\varepsilon < 0$ correspond to the stretching and shrinking parameter respectively). The physical quantities that are used in the present study are the skin friction coefficient and Nusselt number given by

$$C_f = \frac{2\tau_w}{\rho U_e^2} = Re_x^{-1/2} f''(0), \tag{11}$$

$$Nu_x = \frac{xq_w}{k(T_w - T_\infty)} = -Re_x^{1/2}\theta'(0), \tag{12}$$

respectively where $\tau_w = \mu \left(\frac{\partial u}{\partial y}\right)_{y=0}$ is the wall shear stress along the streching/shrinking surface and $q_w = -k \left(\frac{\partial T}{\partial y}\right)_{y=0}$ is the surface heat flux.

B. Stability Analysis

Following (Merkin, 1986), the unsteady case for equations (2) and (3) are considered such that

$$\frac{\partial u}{\partial t} + u\frac{\partial u}{\partial x} + v\frac{\partial u}{\partial y} = U_e\frac{dU_e}{dx} + \nu\frac{\partial^2 u}{\partial y^2} - \frac{\sigma {B_0}^2}{\rho}(u - U_e) + g\beta_T(T - T_\infty), \tag{13}$$

$$\frac{\partial T}{\partial t} + u\frac{\partial T}{\partial x} + v\frac{\partial T}{\partial y} = \alpha\frac{\partial^2 T}{\partial y^2} + \frac{Q}{\rho C_p}(T - T_\infty). \tag{14}$$

The following new non-dimensional variables have been introduced where τ represents the dimensionless time.

$$\eta = \sqrt{\frac{U_e}{\nu x}}y, \qquad f(\eta,\tau) = \frac{\psi}{\sqrt{U_e \nu x}}, \qquad \theta(\eta,\tau) = \frac{T - T_\infty}{T_w - T_\infty}, \qquad \tau = bt, \qquad u = bx\frac{\partial f}{\partial \eta}(\eta,\tau) \quad \text{and} \quad v = -\sqrt{b\nu}f(\eta,\tau) \tag{15}$$

Using (15), Equations (2) and (3) can be written as

$$\frac{\partial^3 f}{\partial \eta^3} + f\frac{\partial^2 f}{\partial \eta^2} - \left(\frac{\partial f}{\partial \eta}\right)^2 - \frac{\partial^2 f}{\partial \eta \partial \tau} + M\left(1 - \frac{\partial f}{\partial \eta}\right) + 1 + \lambda\theta = 0, \tag{16}$$

$$\frac{1}{Pr}\frac{\partial^2 \theta}{\partial \eta^2} + f\frac{\partial \theta}{\partial \eta} - \theta\frac{\partial f}{\partial \eta} - \frac{\partial \theta}{\partial \tau} + S\theta = 0, \tag{17}$$

with the boundary conditions

$$f(0,\tau) = 0, \qquad \frac{\partial f}{\partial \eta}(0,\tau) = \varepsilon, \qquad \theta(0,\tau) = 1, \qquad \frac{\partial f}{\partial \eta}(\eta,\tau) \to 1, \qquad \theta(\eta,\tau) \to 0 \quad \text{as} \quad \eta \to \infty \tag{18}$$

The following representation is adopted to test the stability of the dual solutions according to (Weidman et al., 2006):

$$f(\eta,\tau) = f_0(\eta) + e^{-\gamma\tau}F(\eta,\tau), \qquad \theta(\eta,\tau) = \theta_0(\eta) + e^{-\gamma\tau}G(\eta,\tau), \tag{19}$$

where γ is an unknown eigenvalue parameter, $f(\eta) = f_0(\eta)$, $\theta(\eta) = \theta_0(\eta)$, $F(\eta)$ and $G(\eta)$ are small relative to $f_0(\eta)$ and $\theta_0(\eta)$ respectively. The following linearized problem will be obtained by substituting (19) into (16) and (17):

$$\frac{\partial^3 F}{\partial \eta^3} + f_0\frac{\partial^2 F}{\partial \eta^2} + {f_0}''F - (2{f_0}' - \gamma + M)\frac{\partial F}{\partial \eta} - \frac{\partial^2 F}{\partial \eta \partial \tau} + \lambda G = 0, \tag{20}$$

$$\frac{1}{Pr}\frac{\partial^2 G}{\partial \eta^2} + F{\theta_0}' + f_0\frac{\partial G}{\partial \eta} - \theta_0\frac{\partial F}{\partial \eta} - G{f_0}' - \frac{\partial G}{\partial \tau} + (\gamma + S)G = 0, \tag{21}$$

subject to the boundary conditions

$$F(0,\tau) = 0, \qquad \frac{\partial F}{\partial \eta}(0,\tau) = 0, \qquad G(0,\tau) = 0, \qquad \frac{\partial F}{\partial \eta}(\eta,\tau) \to 0, \qquad G(\eta,\tau) \to 0 \quad \text{as} \quad \eta \to \infty \tag{22}$$

By setting $\tau = 0$, the solutions $f(\eta) = f_0(\eta)$ and $\theta(\eta) = \theta_0(\eta)$ of the steady equations (8) and (9) are obtained. The functions $F(\eta) = F_0(\eta)$ and $G(\eta) = G_0(\eta)$ in (20) and (21) will identify initial growth or decay of the solution (19). Thus the linearized eigenvalue problem are given by

$${F_0}''' + f_0{F_0}'' + {f_0}''F_0 - (2{f_0}' - \gamma + M){F_0}' + \lambda G_0 = 0, \tag{23}$$

$$\frac{1}{Pr}{G_0}'' + F_0{\theta_0}' + f_0{G_0}' - \theta_0{F_0}' - G_0{f_0}' + (\gamma + S)G_0, \tag{24}$$

along with the new boundary conditions

$${F_0}(0) = 0, \qquad {F_0}'(0) = 0, \qquad G_0(0) = 0, \qquad {F_0}'(\eta) \to 0, \qquad G_0(\eta) \to 0 \quad \text{as} \quad \eta \to \infty \tag{25}$$

According to (Harris et al., 2009), the range of possible eigenvalues can be obtained by relaxing a boundary condition on ${F_0}'(\eta)$ or $G_0(\eta)$. In the present study, ${F_0}'(\eta) \to 0$ as $\eta \to \infty$

is relaxed and replaced with the normalizing boundary condition $F_0''(0) = 1$.

III. Results and Discussion

The system of nonlinear ordinary differential equations (8)-(9) subject to the boundary conditions (10) were solved numerically using bvp4c function in Matlab. The results showed the influence of the non-dimensional governing parameters, which are the magnetic parameter M, shrinking parameter ε and mixed convection parameter λ on velocity and temperature profiles as well as the skin friction coefficient and the local Nusselt number. Results are validated from their profiles that asymptotically satisfying the far field boundary conditions. A comparison have also been made to the earlier published results as tabulated in Tables 1 and 2 to validate the accuracy of the numerical results.

Figures 2 and 3 illustrate the variations of

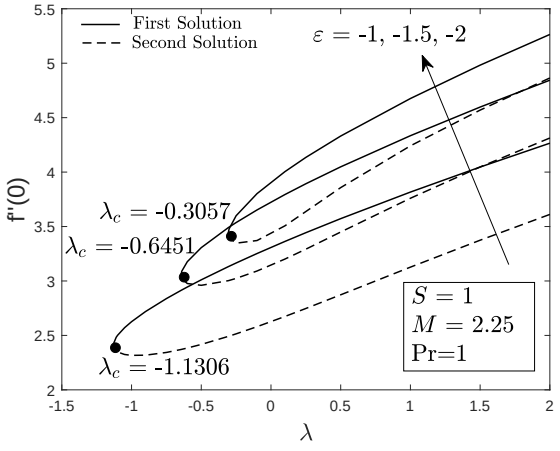

Figure 2: Skin friction coefficient, $f''(0)$ towards mixed convection parameter, λ for various values of shrinking parameter, ε.

the skin friction coefficient and the local Nusselt number towards the mixed convection or buoyancy parameter, λ. These figures present that the dual solutions exist for both assisting flow ($\lambda > 0$) and opposing flow ($\lambda < 0$) up to a critical value λ_c where the solutions do not

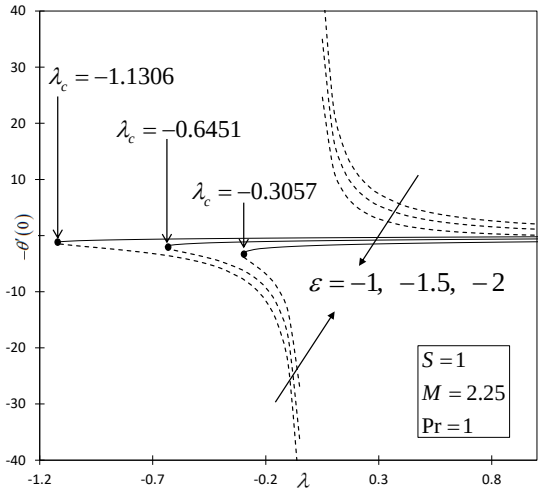

Figure 3: Local Nusselt number, $-\theta'(0)$ towards mixed convection parameter, λ for various values of shrinking parameter, ε.

exist for $\lambda < \lambda_c$. It means that the boundary layer separation occur when $\lambda < \lambda_c$ and full Navier-Stokes equations with energy equation are needed to be solved to observe the behaviour of the flow. In the study, λ for the assisting flow is chosen up to $\lambda = 1$ only and no further investigation is done for $\lambda > 1$. Figure 2 also shows that the dual solutions have positive skin friction coefficient which indicates that the fluid exerts a drag force on the wall and increase as the shrinking parameter increase ($\varepsilon = -1, -1.5, -2$). The local Nusselt number for the first solution decreases slightly as the shrinking parameter increases while the second solution have opposite trend for both flows as shown in Fig. 3. It also can be seen from Figs. 2 and 3 that the value of $|\lambda_c|$ increases as the shrinking parameter decreases ($\varepsilon = -2, -1.5, -1$) and smaller values of ε might be needed and important to delay the boundary layer separation.

In contrast, variations of the skin friction coefficient and the local Nusselt number towards the shrinking parameter, ε for selected values of mixed convection parameter ($\lambda = -0.25, -0.5, -1$) are presented in Figs. 4 and 5. Both figures reveal that reducing the

Table 1: Comparison result of $f''(0)$ and $-\theta'(0)$ for different values of Pr when $\lambda = 1$, $M = 0$, $\varepsilon = 0$ and $S = 0$.

Pr	(Ishak et al., 2008)		(Ali et al., 2014)		(Sharma et al., 2018)		Present	
	$f''(0)$	$-\theta'(0)$	$f''(0)$	$-\theta'(0)$	$f''(0)$	$-\theta'(0)$	$f''(0)$	$-\theta'(0)$
1	1.6754	0.8708	1.6754	0.8708	1.67550	0.87070	1.675436	0.870778
100	1.3680	4.2116	1.3680	4.2133	1.36800	4.21163	1.368034	4.211645

Table 2: Comparison result of $f''(0)$ and $-\theta'(0)$ for assisting flow case ($\lambda = 0.5$) and opposing flow case ($\lambda = -0.5$) with different values of ε when $Pr = 1$, $M = 2.25$ and $S = 1$.

ε	Assisting flow ($\lambda = 0.5$)				Opposing flow ($\lambda = -0.5$)			
	(Sharma et al., 2018)		Present		(Sharma et al., 2018)		Present	
	$f''(0)$	$-\theta'(0)$	$f''(0)$	$-\theta'(0)$	$f''(0)$	$-\theta'(0)$	$f''(0)$	$-\theta'(0)$
0.5	1.21017	0.60290	1.21012	0.60334	0.85009	0.53950	0.85012	0.53973
1.5	-1.00018	1.01315	-1.00026	1.01389	-1.30080	0.97757	-1.30072	0.97828
3.0	-5.09124	1.49900	-5.09133	1.49993	-5.33833	1.48080	-5.33832	1.48093

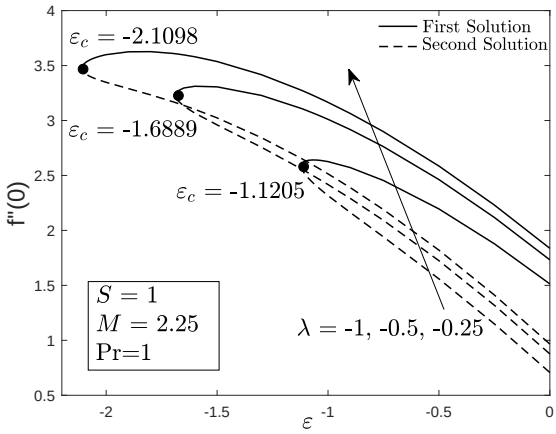

Figure 4: Skin friction coefficient, $f''(0)$ towards shrinking parameter, ε for various values of mixed convection parameter, λ.

values of $|\lambda|$ will increase the value of $|\varepsilon_c|$ and this support the results obtained in Figs. 2 and 3. Meanwhile, Fig. 4 depicts that the positive skin friction coefficient for both first and second solutions decrease as the $|\lambda|$ increases. For the opposing flow case ($\lambda = -0.25, -0.5, -1$), the opposed buoyancy force will reduce the fluid velocity, hence the wall shear stress and the skin friction coefficient will also be reduced. A small reduction of the local Nusselt number from the first solution is noticed as $|\lambda|$ increases, but a significant reduction of it is observed from the second solution. This observation manifest that the opposing buoyant flow will lead to an adverse pressure gradient which will decelerate the fluid flow, hence decrease the wall heat transfer rate.

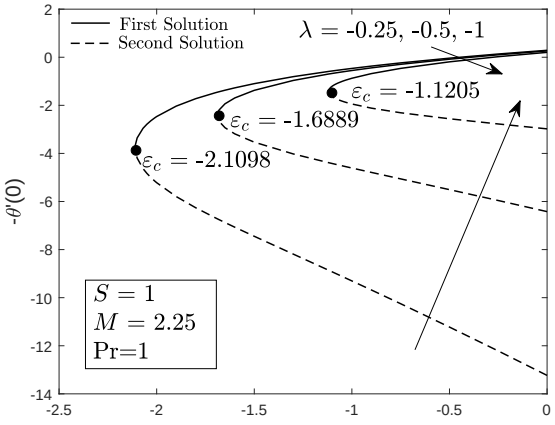

Figure 5: Local Nusselt number, $-\theta'(0)$ towards shrinking parameter, ε for various values of mixed convection parameter, λ.

Figures 6-9 show the effects of magnetic parameter M on the dimensionless velocity and temperature profiles for buoyancy added case

($\lambda = 0.5$) and buoyancy opposed case ($\lambda = -0.5$). The first solution for both velocity profiles (assisting and opposing flow) increase with the increment of the magnetic parameter while reverse effect can be seen from the second solutions. Magnetic field generally produces a drag known as the Lorentz force which decelerates the motion of the fluid in boundary layer, but in the case when free stream velocity start dominating the stretching/shrinking velocity of the surface, there is an opposite effect of magnetic parameter as reported by (Sharma et al., 2018). This motion also might be caused by the buoyancy effect which always increases the momentum boundary layer leading to the increment of velocity distribution. Different temperature profiles were obtained for both flows as can be seen in Figs. 8 and 9. Dual solutions of the assisting flow show a reduction in the thermal boundary layer while for the opposing flow case only first solution decreases as the magnetic parameter increases.

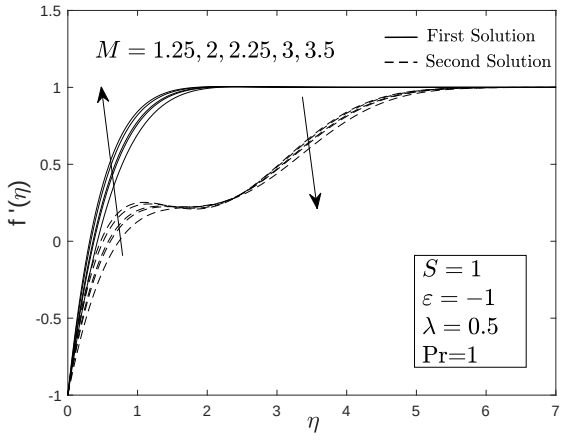

Figure 6: Velocity profile of assisting flow for various values of magnetic parameter, M.

Figure 10 clearly demonstrates that the fluid velocity increases with the increasing values of λ from the first solution while opposite result obtained from the second solution. Figure 11 depicts that as the mixed convection parameters increase, the fluid temperature decreases for the first solution while for the second solution, the result of assisting flow ($\lambda = 0.5, 1$) is

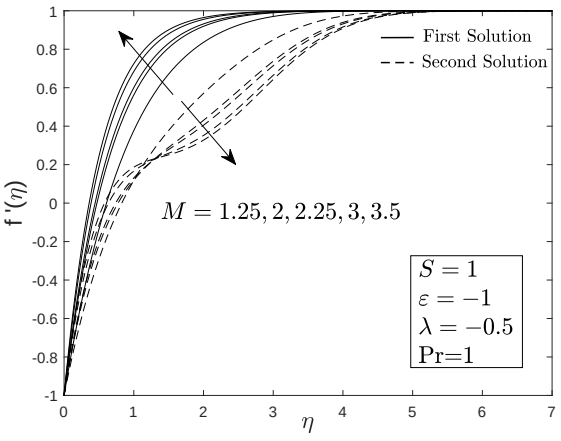

Figure 7: Velocity profile of opposing flow for various values of magnetic parameter, M.

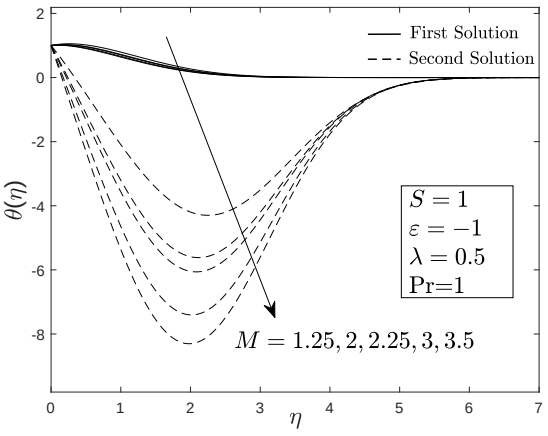

Figure 8: Temperature profile of assisting flow for various values of magnetic parameter, M.

different from the result of the opposing flow ($\lambda = -0.5, -1$).

A stability analysis has been performed using bvp4c function in Matlab to test the stability of the dual solutions found in the study. The flow is not stable if the smallest eigenvalue, γ_1 is negative which indicates that an initial growth of disturbances occur while positive value of the smallest eigenvalue indicates that the flow is stable and physically realizable. The smallest eigenvalue for several values of λ and ε are tabulated in Tables 3 and 4. As shown in the Tables 3 and 4, positive

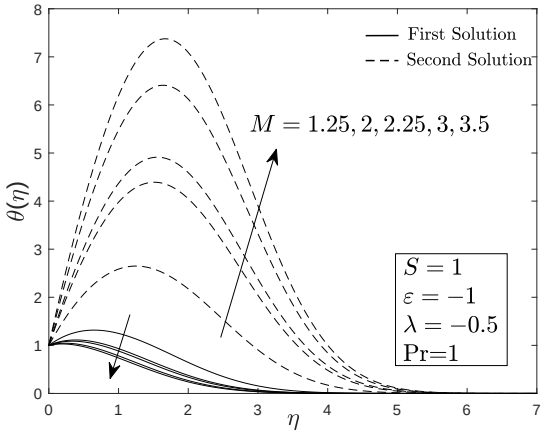

Figure 9: Temperature profile of opposing flow for various values of magnetic parameter, M.

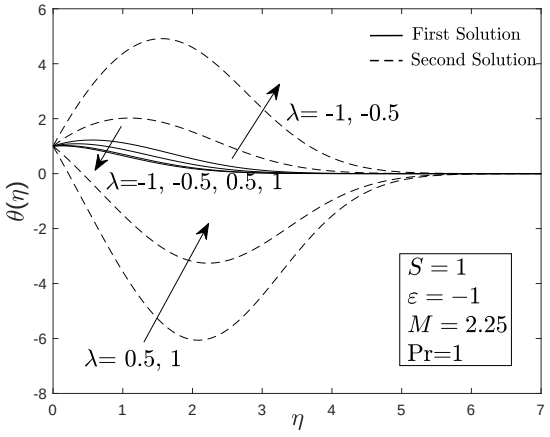

Figure 11: Temperature profile for different values of mixed convection parameter, λ.

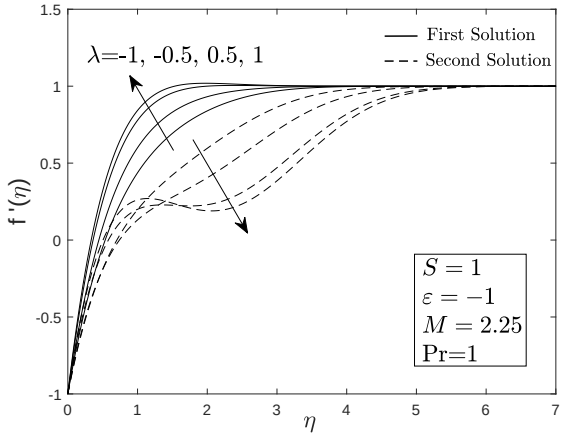

Figure 10: Velocity profile for different values of mixed convection parameter, λ.

values of γ_1 are found for the first solution while negative values of γ_1 are obtained for the second solution which concludes that the first solution is stable and acceptable in this study. From these results, $\gamma_1 \to 0$ as $\varepsilon \to \varepsilon_c$ and $\gamma_1 \to 0$ as $\lambda \to \lambda_c$ for both first and second solution which is consistent with the study by (Merkin, 1986) and (Weidman et al., 2006).

IV. Conclusion

In the present paper, the MHD mixed convective with heat source past a shrinking sheet is investigated. The governing of non-linear partial differential equations are transformed into a system of ordinary differential equations using the similarity transformations and then solved numerically using the bvp4c function in Matlab. The conclusions are:

- Dual solutions are obtained for both assisting flow ($\lambda > 0$) and opposing flow ($\lambda < 0$) within the specific range of mixed convection parameter and shrinking parameter. Since no solutions exist for $\lambda < \lambda_c$ and $\varepsilon < \varepsilon_c$, the full Navier-Stokes and energy equations are needed to be solved to observe the flow behaviour.
- The value of $|\lambda_c|$ increases with the decreasing values of the shrinking parameter while the value of $|\varepsilon_c|$ increases with the decreasing values of the mixed convection parameter for the opposing flow. Boundary layer separation can be controlled or delayed by manipulating these parameters.
- A stability analysis has proven that the upper branch/first solution are physically stable and realizable whereas the lower branch/second solution are not stable .

Table 3: Smallest eigenvalue, γ_1 at several values of ε and λ when $Pr = 1, M = 2.25$ and $S = 1$.

ε	λ	γ_1 (First Solution)	γ_1 (Second Solution)
	-1.1306	0.00473	-0.00473
-1	-1.13	0.02474	-0.02462
	-1.1	0.17635	-0.16920
	-0.6451	0.00006	-0.00072
-1.5	-0.64	0.07577	-0.07424
	-0.6	0.22943	-0.21582
	-0.3057	0.00402	-0.00402
-2	-0.305	0.03064	-0.03034
	-0.3	0.08752	-0.08511

Table 4: Smallest eigenvalue, γ_1 at several values of λ and ε when $Pr = 1, M = 2.25$ and $S = 1$.

λ	ε	γ_1 (First Solution)	γ_1 (Second Solution)
	-2.1098	0.0063	-0.0063
-0.25	-2.109	0.0238	-0.0236
	-2.1	0.0813	-0.0791
	-1.1689	0.0051	-0.0051
-0.5	-1.68	0.0873	-0.0851
	-1.6	0.2828	-0.2618
	-1.1205	0.0007	-0.0009
-1	-1.12	0.023	-0.0229
	-1.1	0.1494	-0.1441

- Fluid velocity increases with the increasing values of magnetic parameter and mixed convection parameter for both assisting and opposing flow.
- Fluid temperature decreases with the increasing values of magnetic parameter and mixed convection parameter for both assisting and opposing flow.

Acknowledgements

The present work is supported by the Universiti Putra Malaysia through the Putra Grant (9570600) and grant GP-IPS/2018/9624700. The main author also would like to acknowledge Ministry of Education (Malaysia) and Universiti Teknikal Malaysia Melaka for the financial support through UTEM-SLAB scholarship. The authors also appreciate the valuable feedbacks and recommendations by the competent reviewers.

References

[1] F. M. Ali, R. Nazar, N. M. Arifin, and I. Pop. Mixed convection stagnation-point flow on vertical stretching sheet with external magnetic field. *Applied Mathematics and Mechanics*, 35(2):155–166, 2014.

[2] I. S. Awaludin, P. D. Weidman, and A. Ishak. Stability analysis of stagnation-point flow over a stretching/shrinking sheet. *AIP Advances*, 6(4):045308, 2016.

[3] T. C. Chiam. Stagnation-point flow towards a stretching plate. *Journal of*

the physical society of Japan, 63(6):2443–2444, 1994.

[4] N. F. Fauzi, S. Ahmad, and I. Pop. Stagnation point flow and heat transfer over a nonlinear shrinking sheet with slip effects. *Alexandria Engineering Journal*, 54(4):929–934, 2015.

[5] S. D. Harris, D. B. Ingham, and I. Pop. Mixed convection boundary-layer flow near the stagnation point on a vertical surface in a porous medium: Brinkman model with slip. *Transport in Porous Media*, 77(2):267–285, 2009.

[6] K. Hiemenz. Die grenzschicht an einem in den gleichformigen flussigkeitsstrom eingetauchten geraden kreiszylinder. *Dinglers Polytech. J.*, 326:321–324, 1911.

[7] F. Homann. Der einfluss grosser zähigkeit bei der strömung um den zylinder und um die kugel. *ZAMM-Journal of Applied Mathematics and Mechanics/Zeitschrift für Angewandte Mathematik und Mechanik*, 16(3):153–164, 1936.

[8] S. S. P. M. Isa, N. M. Arifin, R. Nazar, N. Bachok, F. M. Ali, and I. Pop. Mhd mixed convection boundary layer flow of a casson fluid bounded by permeable shrinking sheet with exponential variation. *Scientia Iranica. Transaction B, Mechanical Engineering*, 24(2):637, 2017.

[9] A. Ishak, R. Nazar, and I. Pop. Mixed convection boundary layers in the stagnation-point flow toward a stretching vertical sheet. *Meccanica*, 41(5):509–518, 2006.

[10] A. Ishak, R. Nazar, N. M. Arifin, and I. Pop. Dual solutions in mixed convection flow near a stagnation point on a vertical porous plate. *International Journal of Thermal Sciences*, 47(4):417–422, 2008.

[11] A. Ishak, K. Jafar, R. Nazar, and I. Pop. Mhd stagnation point flow towards a stretching sheet. *Physica A: Statistical Mechanics and its Applications*, 388(17): 3377–3383, 2009.

[12] A. Jamaludin, R. Nazar, and I. Pop. Three-dimensional mixed convection stagnation-point flow over a permeable vertical stretching/shrinking surface with a velocity slip. *Chinese Journal of Physics*, 55(5):1865–1882, 2017.

[13] T. R. Mahapatra and A. S. Gupta. Magnetohydrodynamic stagnation-point flow towards a stretching sheet. *Acta Mechanica*, 152(1-4):191–196, 2001.

[14] T. R. Mahapatra and A. S. Gupta. Heat transfer in stagnation-point flow towards a stretching sheet. *Heat and Mass transfer*, 38(6):517–521, 2002.

[15] T. R. Mahapatra, S. K. Nandy, and A. S. Gupta. Momentum and heat transfer in mhd stagnation-point flow over a shrinking sheet. *Journal of Applied Mechanics*, 78(2):021015, 2011.

[16] J. H. Merkin. On dual solutions occurring in mixed convection in a porous medium. *Journal of engineering Mathematics*, 20 (2):171–179, 1986.

[17] D. Pal. Heat and mass transfer in stagnation-point flow towards a stretching surface in the presence of buoyancy force and thermal radiation. *Meccanica*, 44(2):145–158, 2009.

[18] H. Rosali, A. Ishak, and I. Pop. Stagnation point flow and heat transfer over a stretching/shrinking sheet in a porous medium. *International Communications in Heat and Mass Transfer*, 38(8):1029–1032, 2011.

[19] G. S. Seth, A. K. Singha, M. S. Mandal, A. Banerjee, and K. Bhattacharyya. Mhd stagnation-point flow and heat

transfer past a non-isothermal shrinking/stretching sheet in porous medium with heat sink or source effect. *International Journal of Mechanical Sciences*, 134:98–111, 2017.

[20] P. R. Sharma, S. Sinha, R. S. Yadav, and A. N. Filippov. Mhd mixed convective stagnation point flow along a vertical stretching sheet with heat source/sink. *International Journal of Heat and Mass Transfer*, 117:780–786, 2018.

[21] M. Shen, F. Wang, and H. Chen. Mhd mixed convection slip flow near a stagnation-point on a nonlinearly vertical stretching sheet. *Boundary Value Problems*, 2015(1):78, 2015.

[22] G. Singh and P. R. Sharma. Heat and mass transfer in the boundary layer flow along a vertical isothermal reactive plate near stagnation point: Existence of dual solution. *Journal of Applied Fluid Mechanics*, 7(1), 2014.

[23] C. Y. Wang. Stagnation flow towards a shrinking sheet. *International Journal of Non-Linear Mechanics*, 43(5):377–382, 2008.

[24] P. D. Weidman, D. G. Kubitschek, and A. M. J. Davis. The effect of transpiration on self-similar boundary layer flow over moving surfaces. *International journal of engineering science*, 44(11-12): 730–737, 2006.